Substitution and Elimination Reaction of F⁻ with C₂H₅Cl: An ab Initio Molecular Dynamics Study

## Martina Mugnai, Gianni Cardini,* and Vincenzo Schettino

Dipartimento di Chimica and European Laboratory for Nonlinear Spectroscopy (LENS), Università di Firenze, Via della Lastruccia 3, 50019 Sesto Fiorentino (Firenze), Italy

The reaction between the fluoride ion and chloroethane has been analyzed by ab initio molecular dynamics. The energy profile and the stationary points for the E2 and S_N2 competing reactions have been characterized. Potential energy surface exploration at 300 K in the Blue Moon ensemble has shown that the two reaction pathways are connected. Some insight on the branching ratio as a function of the temperature has been obtained by analyzing impact trajectories.

I. Introduction

Bimolecular nucleophilic substitution reactions of the type $CH_3X + Y^-$ are of considerable interest as model systems of more complex organic reactions and have been extensively investigated both experimentally[1,2] and theoretically.[3−15] Recently, we have reported[16] on a finite temperature ab initio Car−Parrinello molecular dynamics[17−21] study of the $CH_3Cl + F^-$ reaction using the exchange correlation functional provided by Hamprecht, Cohen, Tozer, and Handy (HCTH).[22,23] Although the level of theory that is necessary to adopt in this ab initio approach is characterized by well-known limitations for S_N2 reactions,[8,14,15,24] the careful exploration of the phase space in the simulation gave evidence for a region connected to a possible pathway for the elimination reaction. The thorough exploration of the phase space allowed by ab initio simulation methods is even more important for the more complex reaction of the fluoride ion with chloroethane:

$$CH_3CH_2Cl + F^- \tag{1}$$
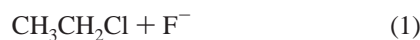
In fact, in this case, the presence of acidic hydrogens brings about a competition between the substitution and elimination reactions.[25−31] In addition, the reduced symmetry of the substrate no longer allows for a straightforward identification of the minimum-energy reaction pathway and requires a more extensive exploration of the potential energy surface.[32,33]

Simple reactions such as the one considered in the present work can be studied in the gas phase in the absence of interactions with neighboring molecules or ions using mass spectrometric detection techniques.[34−41] Unfortunately, for reaction 1, the substitution and elimination reactions produce different neutral species but the same anion

S_N2 products:　　　$CH_3CH_2F + Cl^-$ 　　　(2)

E_2 products:　　　$CH_2{=}CH_2 + HF + Cl^-$ 　　(3)
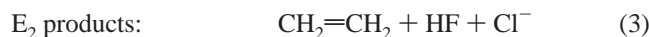
and it is not possible to distinguish between the two processes by the usual spectrometric techniques. The reaction has been studied by Lieder et al.,[34] who analyzed the neutral species fragmentation after the reaction. However, it has been found that the fragmentation of the neutral species gives common products for the two processes; therefore, it was not possible to obtain clear data on the branching ratio for the reaction. Subsequently, DePuy et al.[39] have found the efficiency of this reaction to be higher than that of CH_3Cl with F^-, suggesting the presence of a competing E2 mechanism, but they did not report on the branching ratio either. A new technique to solve this problem and to study the substitution/elimination competition for a few reactions has been successfully introduced by Gronert et al.,[42,43] but it has not been applied to reaction 1.

Ab initio calculations[44,45] have been reported for reaction 1, and several problems have been raised. The elimination reaction involves the breaking and formation of four chemical bonds through a process that is concerted but not necessarily synchronized. Therefore, more transition states should be accessed along the reaction pathway. In addition, the elimination reaction may occur through the anti or syn mechanism, although in the present case the former seems to be favored. There are open questions concerning the structure of the prereactive complex as well. Minato et al.[44] found two distinct minima for the prereactive complex of the S_N2 and E2 reactions, with the fluoride ion closer to the α or β hydrogens, respectively. On the contrary, Gronert,[45] by higher level of calculations, found a single minimum with the fluoride ion almost equidistant from the α and β positions. Finite temperature effects could likewise influence the energetics of the pathways differently, but these effects have not been investigated so far.

In the present paper, we report on Car−Parrinello ab initio molecular dynamics simulations for reaction 1. The calculations have been carried both at ~0 and 300 K, and the energy profiles have been computed in the Blue Moon ensemble, characterizing the reaction pathways of the substitution and elimination processes at finite temperature. To analyze nonequilibrium situations, ab initio impact trajectories have been studied. It will be shown that, depending on the impact geometry, the fluoride initial velocity can affect the two reaction mechanisms differently.

II. Computational Details

The simulations have been performed with the CPMD[46] program in a cubic box with a 25-au side, considering the system to be isolated and solving Poisson's equation by the Barnett

---

Substitution/Elimination of F⁻ with C₂H₅Cl

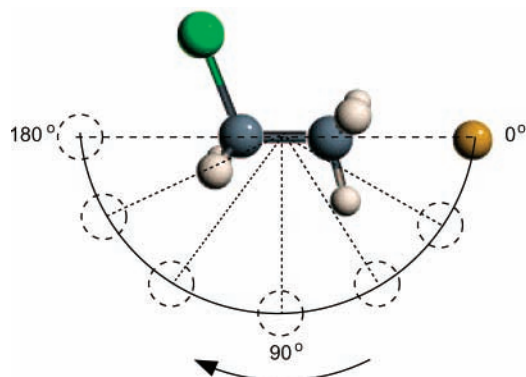*J. Phys. Chem. A, Vol. 107, No. 14, 2003* **2541**

Figure 1. Initial position of the F⁻ ion in the impact trajectories at 700, 1700, and 3000 K, as reported in Table 5.

and Landman implementation of the Hockney method.[47,48] The nuclei and the core electrons of all of the atoms were described by using Troullier–Martins pseudopotentials[49] along with the Kleinman–Bylander decomposition,[50] whereas the valence electronic wave functions were expanded in plane waves with a 70-Ry cutoff. These conditions allow the geometrical parameters to converge to better than 3%. The empirical exchange-correlation functional obtained by Hamprecht et al.[22,23] fitting the 120 system and hereafter denoted as HCTH has been adopted.

Only reaction paths with the F⁻ ion initially on the opposite side of the Cl atom have been considered. This is an obvious choice for the S_N2 reaction and a reasonable one in the case of the E2 reaction. In fact, it is well known that in the gas phase the E2 anti mechanism is significantly favored over the syn mechanism.[45,27] The stationary points along the two reaction paths have been characterized at ~0 K using the HCTH functional. The S_N2 transition state has been determined, starting from the structure suggested by Gronert,[45] by constrained annealing (imposing a bond constraint on the C–Cl and C–F distances) followed by geometry optimization performed by a quasi-Newton method (BFGS).[51] The pre- and postreactive minimum structures have been obtained by an annealed dynamics starting from the S_N2 transition state (TS). The E2 stationary points have been obtained by the geometry optimization of structures taken from the Blue Moon ensemble simulations[52–55] that have been used for a sampling of the phase space.

For the simulations in the Blue Moon ensemble, the $C_α$–Cl or the $C_α$–F distance was maintained at a constant value, and the average temperature was kept at ~300 K by the Nosè–Hoover[56–58] chain algorithm with a bath frequency of 1500 cm⁻¹. The incoming F⁻ ion was set at an anti position with respect to chlorine and at about 4 Å from the center of the C–C bond as shown in Figure 1. Different initial velocities were assigned to the ion.

All of the energies have been referred to the isolated CH₃CH₂Cl molecule (−29.49041062 hartrees) and F⁻ ion (−24.20870335 hartrees) energies computed at 0 K under the same conditions.

Calculations of the stationary points have also been performed, by comparison, using standard density functional calculations with the B3LYP functional along with the 6-311G++(d,p) basis set using the Gaussian 98[59](G98) suite of programs and with the same basis set at the second-order Möller Plesset (MP2)[60] level of theory.

III. Results and Discussion

In Table 1, the structural data calculated with the Car–Parrinello method and the HCTH functional for the isolated

TABLE 1: Structural Parameters of Isolated Molecules CH₃CH₂Cl, CH₃CH₂F, and CH₂CH₂

C₂H₅Cl					
distances (Å)	exptl[62]	HCTH	B3LYP	MP2	Minato[44]
C–C	1.528	1.516	1.516	1.517	1.519
C–Cl	1.802	1.801	1.823	1.787	1.904
C–H	1.103	1.096	1.092	1.092	1.086

angles (deg)	exptl[62]	HCTH	B3LYP	MP2	Minato[44]
C–C–Cl	110.7	111.9	111.5	110.9	
$H_α$–$C_α$–$H_α$	109.2	108.7	109.1	108.9	
$H_β$–$C_β$–$H_β$	109.8	108.3	108.2	108.6	
$C_β$–$C_α$–$H_α$	110.6	111.9	112.1	111.3	

C₂H₅F					
distances (Å)	exptl[61]	HCTH	B3LYP	MP2	Minato[44]
C–C	1.5128	1.513	1.512	1.511	1.517
C–F	1.3825	1.407	1.407	1.397	1.438
C–H	1.0949	1.096	1.093	1.092	1.084

angles (deg)	exptl[61]	HCTH	B3LYP	MP2	Minato[44]
$H_α$–$C_α$–$H_α$	108.7	108.8	109.0	109.2	
$H_β$–$C_β$–$H_β$		109.5	108.3	108.8	

C₂H₄				
distances (Å)	exptl[62]	HCTH	B3LYP	MP2
C–C	1.339	1.333	1.333	1.339
C–H	1.087	1.089	1.085	1.085

angles (deg)	exptl	HCTH	B3LYP	MP2
H–C–H		116.5	116.5	117.1
dihedral H–C–C–H		179.9	179.9	179.9

molecules involved in the reaction are reported. The results are in good agreement with experiment[61,62] and are significantly improved in comparison with calculations by Minato et al.[44] performed at a lower level of theory. This is particularly evident for the carbon–halogen bond distances. B3LYP/6-311++G-(d,p) and MP2/6-311++G(d,p) calculations have also been reported for comparison. These calculations are of interest since the B3LYP has been proven to be one of the most accurate exchange correlation functionals in determining equilibrium molecular properties, and the MP2 method gives the simplest correction to the HF method to take electronic correlation into account and is frequently used in studies of chemical reactions.

As found in previous work,[8,14,15,24] the MP2 method gives a shorter C–Cl bond length than DFT calculations. Concerning ethylene, both the HCTH and the B3LYP functionals give perfect agreement with experimental data. The overall agreement in reproducing the structures of the isolated molecules by the HCTH functional is such that it can be used with confidence for at least a semiquantitative study of this reaction, keeping in mind the general tendency of the GGA functional to overstabilize the S_N2 transition states.[63]

The results obtained for the stationary points of the elimination and substitution reactions are reported in Table 2. The search of the stationary points was carried as described in the preceding section. The results are compared with a DFT calculation in a B3LYP/6-311++G(d,p) approach, with an MP2/6-311++G(d,p) calculation, and with the results of Gronert.[45] Controversial results concerning the first prereactive minima have been reported in previous work.[45,44] Two different prereactive complexes for the elimination and substitution reactions have been obtained by Minato et al.[44] using a small basis set, in contrast to Gronert's[45] conclusion of a single prereactive complex for the two reactions. The source of this discrepancy

TABLE 2: Structural Data of the Stationary Points along the Elimination and Substitution Reaction Paths[a]

Prereactive Minimum

	C_α–Cl	C_α–F	C–C	C_β–H_F	C_β–H	F–H	F–C_β–C_α
MP2	1.826	2.856	1.508	1.100	1.095	1.977	74.62
HCTH*	1.899	3.425	1.485	1.168	1.098	1.575	104.2
B3LYP	1.896	3.253	1.494	1.134	1.094	1.688	93.70
ref 45	1.87	2.78	1.51			2.20	

Transition State

substitution

	C_α–Cl	C_α–F	C–C	C_β–H_F	C_β–H	F–H	F–C_β–C_α
MP2	2.210	2.001	1.503	1.090	1.092	2.207	50.37
HCTH	2.200	2.164	1.500	1.097	1.097	2.244	52.90
B3LYP	2.200	2.162	1.498	1.092	1.092	2.199	53.57
ref 45	2.23	2.23	1.50				

elimination

	C_α–Cl	C_α–F	C–C	C_β–H_F	C_β–H	F–H	F–C_β–C_α
MP2	1.999	3.214	1.443	1.433	1.093	1.125	90.64
HCTH	2.049	3.318	1.447	1.274	1.097	1.300	107.4
B3LYP	2.103	3.259	1.438	1.293	1.092	1.281	105.0
ref 45	2.22		1.42	1.34		1.21	

Postreactive Minimum (S_N2)

	C_α–Cl	C_α–F	C–C	C_β–H_F	C_β–H	F–H	F–C_β–C_α
MP2	3.400	1.423	1.507		1.094		33.96
HCTH	3.532	1.439	1.507		1.099		33.79
B3LYP	3.518	1.435	1.520		1.103		33.48

[a] The main differences in spurius S_N2 minima are in the following geometrical parameters: C_α–F = 2.732 Å, F–H = 2.069 Å, F–C_β–C_α = 68.71 Å. The TS imaginary frequency for the E2 and S_N2 mechanisms are, respectively, −557.1 and −344.0 cm^{-1} at the B3LYP level, −746.8 and −569.5 cm^{-1} at the MP2 level, and −382 and −112 cm^{-1} at the HCTH level.

has been clarified by the calculations in the present work. In fact, we have found that both the B3LYP and the MP2 calculations predict a single minimum. The minimum is closer to an S_N2-type or to an E2-type prereactive complex for the two theoretical approaches, respectively. The results are reported in Table 2. However, a single minimum is obtained only when a "very tight" convergence criterion is adopted in the G98[59] calculations. Otherwise, both the B3LYP and MP2 calculations would predict two very close lying minima. The situation is further enlightened by the HCTH calculations. Fulfilling the standard convergence criteria (maximum force $< 5 \times 10^{-4}$ au), two distinct minima were obtained, but in performing further annealing, the S_N2-type minimum moved to coincide with the E2-type minimum. During this annealing, the temperature never exceeded 1 K. This implies that the potential energy surface is flat. Additional evidence for the shape of the energy surface is gained by considering that at both the MP2 and B3LYP levels a number of vibrational frequencies of the prereactive complex are indeed very low. It is evident that these overall results of the structure of the prereactive minimum must be ascribed to the role of dispersive and H-bonding interactions in the various computational approaches.

The TS structure for the S_N2 reaction (see Table 2) shows that the C_α–Cl distance at the HCTH level agrees with the B3LYP result and, contrary to what was found in previous calculations,[14,24] is slightly lower than the MP2 results. The same behavior has been found for C_α–F but to a greater extent. In agreement with the Hammond postulate,[64] the C_α–F bond length is slightly shorter than the C–Cl bond length. The structural results for the E2 TS show, as expected, good agreement
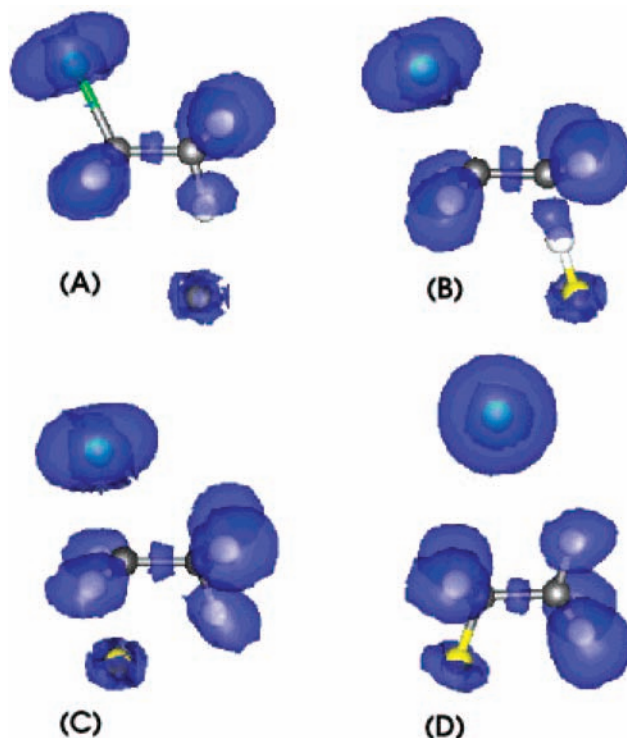

Figure 2. Electron localization functions (ELF) at stationary points of the E2 and S_N2 reactions (isosurface $f = 0.8$). (A) Prereactive minimum. (B) E2 transition state. (C) S_N2 transition state. (D) S_N2 postreactive minimum. ELF funcions have been visualized using the gOpenMol program.[69,70]

between the HCTH and B3LYP calculations, which give longer bond lengths with respect to MP2, especially for the F–H distance. For the transition states of both mechanisms, a single imaginary frequency is found. These are reported in Table 2. It can be seen that the absolute value of the frequency of the E2 TS is considerably higher than for the S_N2 mechanism, implying a steeper energy barrier in the former case.

Electron localization functions (ELF) have been calculated for the stationary points of the two reaction paths and have been represented in a graphical way in Figure 2, where the non-equivalence of the three hydrogens of the methyl group in the prereactive complex due to the interaction with the fluoride ion is evident (see Figure 2A). The electron localization is reduced on the hydrogen closer to the fluoride ion because of the formation of a hydrogen bond. This effect can be also appreciated in the S_N2 transition state.

The nonsynchronous bond breaking/formation in the elimination reaction is highlighted by the transition state ELF function where the bond attractor between the carbon and the hydrogen atoms is still present. In fact, after the F–H bond formation, the C–H bond is not completely broken.

In Table 3, the calculated energies for the prereactive complex and for the TS of the two reactions are reported. It can be seen that the energies calculated with the B3LYP functional are always lower than those calculated with the HCTH functional. This is particularly evident for the S_N2 reaction mechanism, where the largest difference is found for the postreactive complex. From Table 3, it can also be seen that the functional choice affects the various states differently. This should be ascribed to the fact that the HCTH and B3LYP functionals reproduce more accurately the correlation and exchange parts, respectively. As expected on the basis of previous work,[8,14,15,24,63] the MP2 calculations give much higher barriers than DFT for both reactions and, in particular, for the S_N2 substitution. It is

Substitution/Elimination of F⁻ with C₂H₅Cl

J. Phys. Chem. A, Vol. 107, No. 14, 2003 **2543**

TABLE 3: Energies (kJ/mol, with respect to the reactants) of the Stationary Points of the Two Reaction Paths Computed at Different Levels of Theory: MP2/6-311++G(d,p),HCTH/PW and B3LYP/6-311++G(d,p)[a]

	MP2	HCTH	B3LYP
prereactive M.	−69.55	−72.63	−79.41
transition state (E2)	−39.77	−68.9	−71.34
transition state (S_N2)	−20.43	−52.11	−66.79
postreactive M. (S_N2)	−162.03	−167.28	−190.14
barrier (E2)	29.78	3.73	8.07
barrier (S_N2)	49.11	20.49	12.62

[a] The S_N2 barrier is calculated with respect to the prereactive S_N2 spurius minimum: 14.95 kJ/mol.

in fact well established[8,14,15,24,63] that the DFT calculations overstabilize the TS of S_N2 reactions, giving rise to low barriers. On the contrary, calculations at the Hartree−Fock level and, to a lesser extent, MP2 calculations overestimate the barriers for these reactions.

Apart from this, the energy barrier for the substitution reaction is calculated to be higher than for the elimination, independent of the level of theory. This result is in disagreement with previous calculations[44,45] that predict the E2 barrier to be higher than the S_N2 barrier. However, the calculations by Minato[44] are at a much lower level of theory than those used in the present work. The difference with Gronert et al.'s[45] calculations should be ascribed to the adopted procedure that is based on a Möller−Plesset correction applied to HF-level optimized structures. The results obtained in the present work suggest that the E2 mechanism is favored from an energetic point of view. The present results are in agreement with available experimental data. In fact, Lieder and Brauman,[34] on the basis of their IRC measurements, have suggested that S_N2 is the preferred channel, but they have also found products that can be attributed only to the elimination reaction. Strong support for the presence of the E2 mechanism has been given by DePuy et al.[39] The experiments were carried at finite temperature whereas the results reported so far in this work refer to zero temperature. The temperature effects can affect the energetics of the two mechanisms, which has been studied by two different approaches, namely, either by equilibrium simulations at 300 K or by impact studies.

The present calculations show that in both cases the energy of the TS is lower than that of the separated reactants; therefore, the reaction rate could be dominated by the entropy factor even if, as discussed by Wang and Hase,[7] the assumption that the central barrier has no effect on the rate constant is probably not correct in some cases. However, it has been found that the potential well associated with the prereactive complexes and the energy barrier can be significantly higher than kT (particularly at the MP2 level), as can be seen from Table 3. Therefore, trapping in the prereactive minimum is possible, particularly in the low-temperature regime. It is therefore of interest to investigate the energies of the reaction pathways at different temperatures.

A. Thermal Effects. To evaluate the thermal effects on the two reaction paths, a series of simulations have been performed in the Blue Moon ensemble. To evaluate the free energy of the S_N2 reaction, we have constrained either the C_α−Cl or C_α−F bond length, which has been shown to be a suitable choice to analyze substitution reaction paths.[16,65,66]

From the average potential energy as a function of the reaction coordinate $r_{C_\alpha-Cl}-r_{C_\alpha-F}$ reported in Figure 3, we note that for both small and large values of the C_α−Cl distance the curve is very noisy. This is due mainly to the fact that the sampled
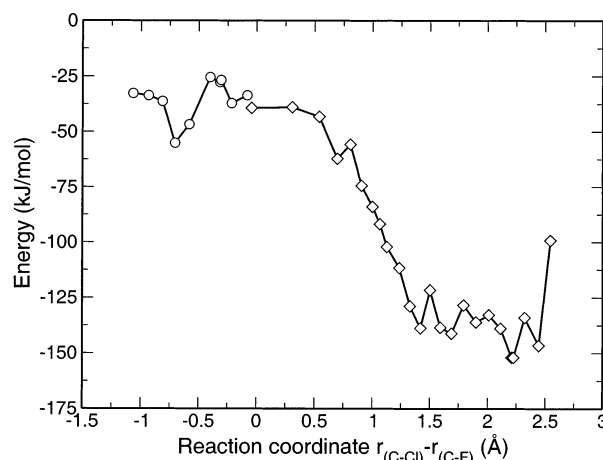

Figure 3. Blue Moon reaction profile as a function of the $r_{C_\alpha-Cl}-r_{C_\alpha-F}$ reaction coordinate obtained by constraining C−F (○) and C−Cl (◇) distances.

configurations belong either to the elimination or substitution pathway. In addition, large uncertainties arise from the methyl rotation. A much clearer picture is gained by reporting the average potential energy corresponding to the phase-space points explored during the Blue Moon trajectories as a function of the difference in the C_α−Cl and C_α−F distances, $r_{C_\alpha-Cl}-r_{C_\alpha-F}$ and the difference in the distances of the fluoride ion from the two carbon atoms, $r_{C_\alpha-F}-r_{C_\beta-F}$ (Figure 4). On the basis of the sign of the last coordinate, it is possible to distinguish between points that more likely belong to the elimination (negative sign) or substitution (positive sign) reaction. It is evident from Figure 4 that the two surfaces are not separated by a high energy barrier, that at 300 K it is possible to move from one reaction mechanism to the other, and that both reaction pathways are accessible. This prevents the evaluation of the free energy associated with the two different reaction paths since it was not possible, with a simple contraint, to explore only one reaction path.

B. Impact Trajectories. Very often, simple reactions do not behave statistically, as shown, for example, for the CH_3Cl + F⁻ reaction.[43,67,68] It is therefore of interest to analyze the possible reaction paths in a nonequilibrium situation as a function of the relative impact velocities to gain some insight into which mechanism is active under different conditions. Impact trajectories have been performed using the HCTH functional. As previously discussed, the S_N2 reaction barrier is higher than the E2 reaction barrier at all levels of theory; therefore, the results of the present HCTH impact studies can be taken with confidence. Because of the high computational resources that are needed to cover all of the possible impact trajectories fully, only two series of impact trajectories were performed to analyze the dependence on the relative impact velocity on one side and the dependence on the impact geometry on the other side.

The first set of ab initio impact trajectories was carried out with several initial velocities of the F⁻ colliding ion, corresponding to a translational temperature in the range between 30 and 3000 K. The choice of the initial ion position can favor one reaction mechanism or the other. Therefore, a starting configuration that can reasonably allow both mechanisms has been selected, locating the fluoride ion in an anti position with respect to the chlorine at 4 Å on the axis perpendicular to the C−C bond. The impact trajectory results are summarized in Table 4 and show that the E2 or the S_N2 reactions are observed at low and high impact velocities, respectively.
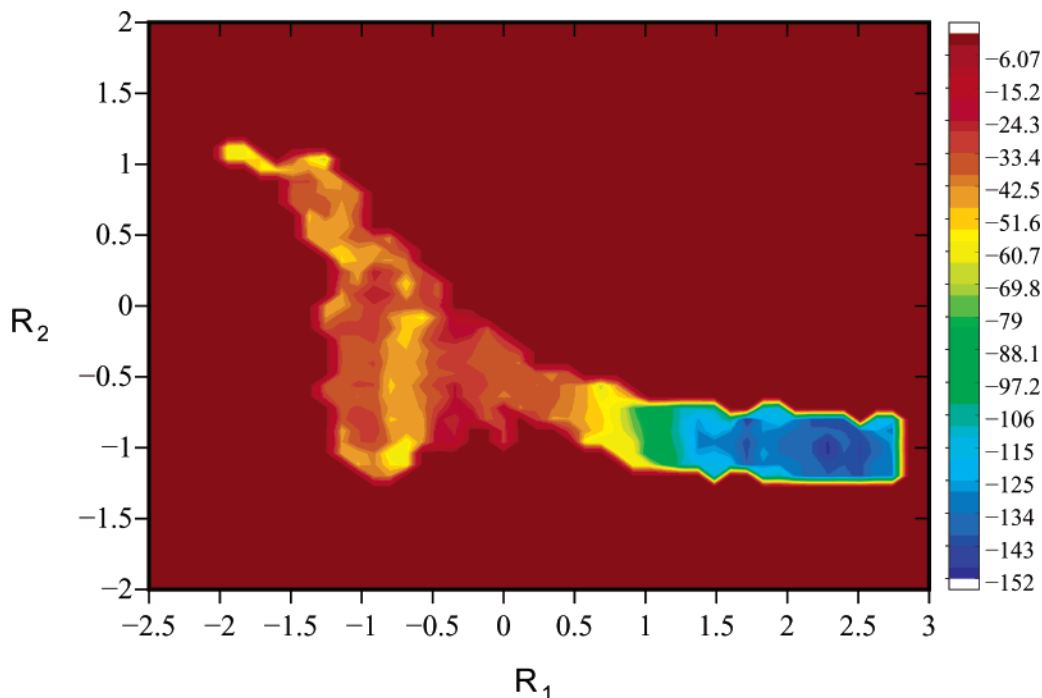
Figure 4. Blue Moon potential energy surface as a function of $r_{C_\alpha-Cl}-r_{C_\alpha-F}$ (R$_1$) and $r_{C_\alpha-F}-r_{C_\beta-F}$ (R$_2$) reaction coordinates. Colors indicate energy values calculated with respect to the reactants in kJ/mol. (See the energy scale in the right-hand side.)

TABLE 4: Results at Different Temperatures for Impacts with the F$^-$ Ion Set at an Initial Distance of 4 Å from the C$-$C Bond Center (90° Position in Figure 1)[a]

temperature (K)	results	mechanism
30	not observed	E2
40	not observed	E2
186	observed	*S$_N$2*, **E2**
333	not observed	*E2, S$_N$2*
422	observed	*S$_N$2*, **E2**
500	observed	*E2, S$_N$2*, **E2**
617	observed	*S$_N$2*, **E2**
720	not observed	S$_N$2
813	not observed	S$_N$2
1024	not observed	S$_N$2
1300	not observed	S$_N$2
1921	not observed	S$_N$2
2432	observed	S$_N$2
2710	observed	S$_N$2
3000	observed	S$_N$2

[a] "Not observed" indicates impact trajectories not leading to final products. Italic font indicates that the fluoride ion is bounced back after having approached the C$_\alpha$ atom (S$_N$2) or a H$_\beta$ (E2) atom.

TABLE 5: Results of Trajectories Studies for Different Impact Angles at Three Different Impact Temperatures[a]

degrees	700 K	1700 K	3000 K	degrees	700 K	1700 K	3000 K
30			E2	90			
45	E2	E2	E2	105	S$_N$2	S$_N$2	S$_N$2
50		E2	E2	110	S$_N$2	S$_N$2	S$_N$2
55	E2	E2		115		S$_N$2	S$_N$2
60	E2			120			S$_N$2
65				125			S$_N$2
75				130			
70				135			
90				150			

[a] See Figure 1 for impact labelling.

A possible explanation can be the found in the impact dynamics. The fluoride ion has to reach a position close to the β hydrogen to activate the elimination mechanism. Since the ion was directed toward the center of the bond, a molecular
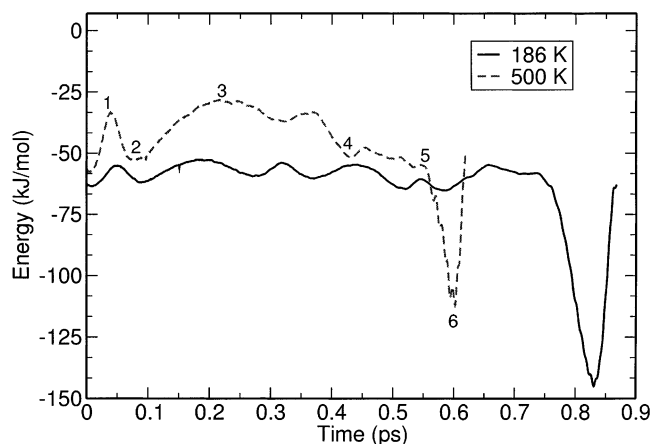

Figure 5. Potential energy as a function of time for the two E2 effective impacts at initial temperatures of 186 ($-$) and 500 K ($--$).

rotation (driven essentially by the ion$-$dipole interaction and by the repulsive interactions of the fluoride ion with the atoms of chloroethane) is necessary to make the E2 reaction mechanism possible. When the impact velocity is low, the molecule has more time to rotate, and the elimination can eventually occur. On the other side, to reach the α carbon for the substitution, the fluoride ion must deeply penetrate into the CH$_2$-Cl umbrella and overcome a significant barrier to reach the prereactive minimum. In Figure 5 and 7, the potential energy profiles of some observed elimination and substitution impacts are reported. All of the profiles are characterized by an initial maximum that does not correspond to a transition state but to a configuration where the fluoride ion approaching the α carbon is subject to the repulsive forces due to the hydrogen atoms. When the temperature is too low, the F$^-$ is bounced back, and the elimination can occur. This is the case of the impact trajectories at 186, 422, 500, and 617 K. This is shown for the 500 K impact trajectory in Figure 6, where selected configurations along the trajectory are reported. It can be seen that high-energy configuration (1) is first reached; then the ion is bounced
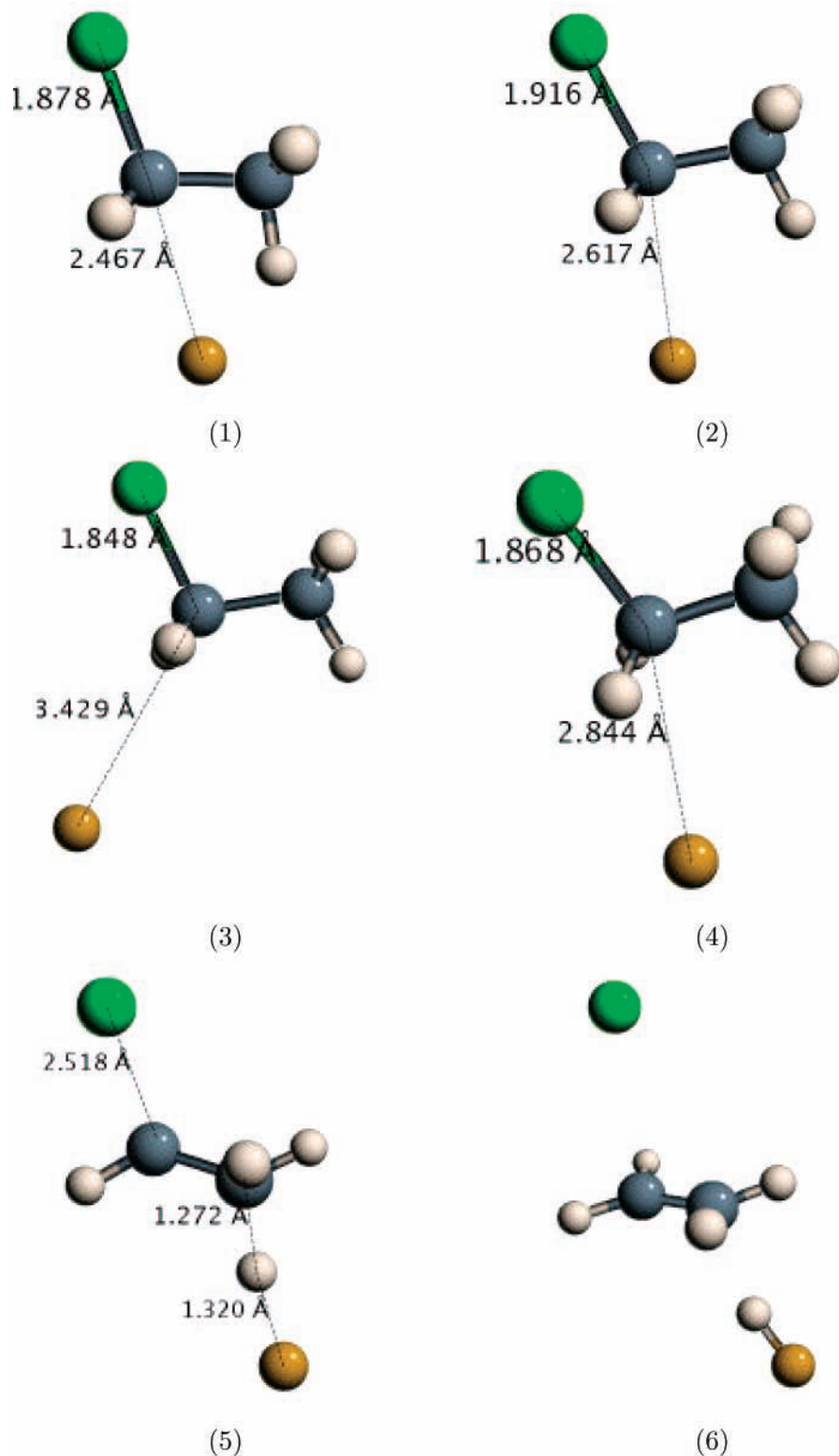
Figure 6. Snapshot of the E2 reaction at 500 K. The numbering refers to the labels along the impact energy profile in Figure 5.

[(2) and (3)], and an ion−molecule reciprocal rotation follows (4), leading to the intermediate structure (5) and finally to the E2 products. This can also be observed by following the H−F distance behavior. (See Figure 8.) The H−F distance decreases while approaching the high-energy configuration, then it increases during the rotation of the molecule to reach a conformation favorable for the elimination. At this point, the H−F distance starts decreasing again and oscillates when the elimination has occurred. This behavior implies that energy is

stored in the H−F bond, and this is also confirmed by the energy distribution analysis (not reported). The 333 K impact is ineffective even if it is in the middle of the E2 range. This is due to CH_3 rotation that prevents the H-bonded complex formation. In Table 6, the C_α−Cl and C_β−F distances for the maximum-energy configuration at various temperatures are reported. A regular decrease in the C_β−F distance with increasing temperature is observed. This shows that when the F⁻ ion with higher velocity can penetrate more deeply into the
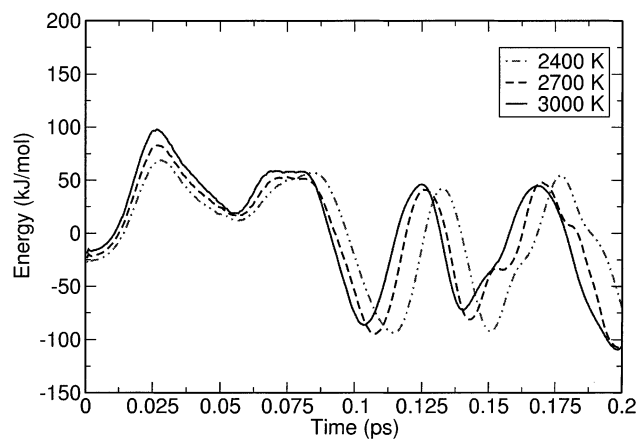
Figure 7. Potential energy as a function of time for three S_N2 effective impacts at initial temperatures of 2400 ($- \cdot \cdot -$), 2700 ($- -$), and 3000 K ($-$).
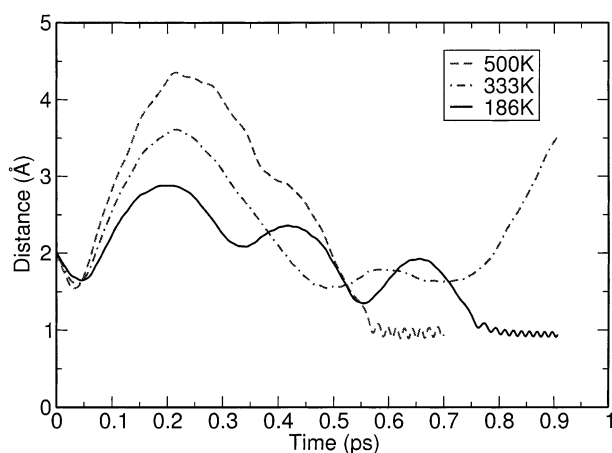

Figure 8. Time evolution of the H$-$F distance for three different impact trajectories at 186, 333, and 500 K, as reported in Table 4.

TABLE 6: C$-$Cl and C$-$F Distances of the Maximum-Energy Configurations of the Observed Impacts in Table 4

temperature (K)	C$-$Cl (Å)	C$-$F (Å)
186	1.878	2.637
422	1.878	2.493
500	1.878	2.467
617	1.899	2.307
2432	1.900	2.125
2710	1.901	2.095
3000	1.902	2.066

hydrogens region and overcome the repulsion the reaction can proceed toward the substitution products.

Because of the high S_N2 impact temperatures, the energy redistribution after the reaction is quite difficult, and the kinetic energy is mainly stored in the chlorine translation with only a small amount distributed in the ethyl fluoride vibrational modes.

The effects of the fluoride ion's initial position on the reaction path have been investigated by performing another series of impact trajectories. The ion has been placed in the plane containing the Cl$-C_\alpha-C_\beta$ angle in the direction of the $C_\alpha-C_\beta$ bond 3 Å from C_β. From this position, the ion has then been rotated (maintaining an anti position with respect to the chlorine) along a semicircle centered in the middle of the $C_\alpha-C_\beta$ bond. (See Figure 1.)

The results for three different impact temperatures (700, 1700, and 3000 K) have been summarized in Table 5. For the impacts at angles around 90°, no reactions have been observed. However,

the reaction can occur by changing the impact angle. Obviously, the E2 reaction is favored for impact angles lower than 90° (F$^-$ close to CH$_3$) whereas the S_N2 reaction is favored for impact angles larger than 90° (F$^-$ on the CH$_2$Cl side). From Table 5, it is possible to analyze the E2/S_N2 ratio at different impact temperatures for this impact series. The E2/S_N2 branching-ratio calculation would require much more statistical analysis, but some qualitative considerations can be made. While the impact temperature increases, the number of times in which the E2 reaction occurs seems to be constant, even though at different impact geometries, while the S_N2 occurrences increase. This does not differ from Gronert's[45] consideration that the E2 reaction is favored from an entropic point of view since our observations are related to a limited number of trajectories on a selected plane. This does not allow us to identify a general trend for the reactivity, but it is useful to show that the cross section of the reaction can be influenced by the initial velocity and position of the ion in a different way for the two reaction paths. It can therefore be argued that the E2/S_N2 ratio decreases with increasing the impact temperature, confirming the results of the 300 K Blue Moon simulation.

IV. Conclusions

In the present work, the competition between E2 and S_N2 mechanisms in the reaction F$^-$ + CH$_3$CH$_2$Cl has been investigated. Energy profiles at ~0 K have been calculated using the HCTH functional. The structure and energy of the stationary points have been compared with results at the B3LYP/6-311++G(d,p) and MP2/6-311++G(d,p) levels of theory. The reported calculations agree in indicating the E2 reaction path to be energetically favored with respect to the S_N2 mechanism at 0 K. Finite temperature calculations in the Blue Moon ensemble show that at 300 K the two potential energy surface are connected, and this implies that in this case an evaluation of the free energy is not possible with this method. Temperature effects on the reaction mechanisms have been investigated by carrying out impact trajectories that shoot the F$^-$ ion toward the middle of the C$-$C bond. In these impacts, E2 and S_N2 reaction mechanisms are favored at low and high temperatures, respectively. The kinetic energy distribution following the E2 reaction shows that vibrational energy is mainly stored in H$-$F stretching whereas after the S_N2 reaction the kinetic energy is mainly transferred to Cl$^-$ ions.

References and Notes

(1) Pellerite, M. J.; Brauman, J. I. *J. Am. Chem. Soc.* **1980**, *102*, 5993−5999.

(2) Pellerite, M. J.; Brauman, J. I. *J. Am. Chem. Soc.* **1983**, *105*, 2672−2680.

(3) Glukhovtsev, M. N.; Pross, A.; Radom, L. *J. Am. Chem. Soc.* **1995**, *117*, 2024−2032.

(4) Glukhovtsev, M. N.; Bach, R.; Pross, A.; Radom, L. *Chem. Phys. Lett.* **1996**, *260*, 558−564.

(5) Botschwina, P.; Horn, M.; Seeger, S.; Oswald, R. *Ber. Bunsen-Ges. Phys. Chem.* **1997**, *101*, 387−390.

(6) Wang, H.; Goldfield, E.; Hase, W. *J. Chem. Soc., Faraday Trans.* **1997**, *93*, 737−746.

(7) Wang, H.; Hase, W. *J. Am. Chem. Soc.* **1997**, *119*, 3093−3102.

(8) Raugei, S.; Cardini, G.; Schettino, V. *J. Chem. Phys.* **1999**, *111*, 10887−10894.

(9) Tachikawa, H.; Igarashi, M. *Chem. Phys. Lett.* **1999**, *303*, 81−86.

(10) Tachikawa, H. *J. Phys. Chem. A* **2000**, *104*, 497−503.

(11) Angel, L.; Ervin, K. M. *J. Phys. Chem A* **2001**, *105*, 4042−4051.

(12) Ensing, B.; Meijer, E.; Blöchl, P. E.; Baerends, E. *J. Phys. Chem. A* **2001**, *105*, 3300−3310.

(13) Sun, L.; Hase, W. L.; Song, K. *J. Am. Chem. Soc.* **2001**, *123*, 5753−5756.

(14) Pagliai, M.; Raugei, S.; Cardini, G.; Schettino, V. *Phys. Chem. Chem. Phys.* **2001**, *3*, 2559−2566.

(15) Pagliai, M.; Raugei, S.; Cardini, G.; Schettino, V. *Phys. Chem. Chem. Phys.* **2001**, *3*, 4870−4873.

(16) Mugnai, M.; Cardini, G.; Schettino, V. *J. Chem. Phys* **2003**, *118*, 2767−2774.

(17) Car, R.; Parrinello, M. *Phys. Rev. Lett.* **1985**, *55*, 2471−2474.

(18) Remler, D.; Madden, P. *Mol. Phys.* **1990**, *70*, 921−966.

(19) Galli, G.; Pasquarello, A. *Computer Simulation in Chemical Physics*; Allen, M. P., Tildesley, D. J., Eds.; Series C: Mathematical and Physical Sciences; Kluwer Academic Publishers: Dordrecht, The Netherlands, 1993; Vol. 397.

(20) Parrinello, M. *Solid State Commun.* **1997**, *102*, 107−120.

(21) Parrinello, M. *Comput. Sci. Eng.* **2000**, *2*, 22−27.

(22) Hamprecht, F. A.; Cohen, A. J.; Tozer, D. J.; Handy, N. C. *J. Chem. Phys.* **1998**, *109*, 6264−6271.

(23) Boese, A. D.; Doltsinis, N. L.; Handy, N. C.; Sprik, M. *J. Chem. Phys.* **2000**, *112*, 1670−1678.

(24) Raugei, S.; Cardini, G.; Schettino, V. *J. Chem. Phys* **2001**, *114*, 4089−4098.

(25) Gronert, S. *J. Am. Chem. Soc.* **1993**, *115*, 652−659.

(26) Bieckelaupt, F. M. *J. Comput. Chem.* **1999**, *20*, 114−128.

(27) Biecklehaupt, F.; Baerends, E.; Nibbering, N.; Ziegler, T. *J. Am. Chem. Soc.* **1993**, *115*, 9160−9173.

(28) Chung, D. S.; Kim, C. K.; Lee, B.; Lee, I. *J. Phys. Chem A* **1997**, *101*, 9097−9104.

(29) Dewar, M. J. S.; Yuan, Y. C. *J. Am. Chem. Soc.* **1990**, *112*, 2088−2094.

(30) Dewar, M. J. S.; Yuan, Y. C. *J. Am. Chem. Soc.* **1990**, *112*, 2095−2105.

(31) Hu, W. P.; Truhlar, D. G. *J. Am. Chem. Soc.* **1996**, *118*, 860−869.

(32) Merrill, G.; Gronert, S.; Kass, S. *J. Phys. Chem. A* **1997**, *101*, 208−218.

(33) Laerdahl, J.; Uggerud, E. *Int. J. Mass Spectrom.* **2002**, *214*, 277−314.

(34) Lieder, C.; Brauman, J. *Int. J. Mass Spectrom. Ion Phys.* **1975**, *16*, 307.

(35) Lum, R. C.; Grabowski, J. J. *J. Am. Chem. Soc.* **1988**, *110*, 8568−8570.

(36) de Koning, L. J.; Nibbering, N. M. M. *J. Am. Chem. Soc.* **1987**, *109*, 1715−1722.

(37) Jones, M. E.; Ellison, B. *J. Am. Chem. Soc.* **1989**, *111*, 1645−1654.

(38) Occhiucci, G.; Speranza, M.; de Koning, L. J.; Nibbering, N. M. *J. Am. Chem. Soc.* **1989**, *111*, 7387−7392.

(39) DePuy, C. H.; Gronert, S.; Mullin, A.; Bierbarum, V. *J. Am. Chem. Soc.* **1990**, *112*, 2095−2105.

(40) Lum, R. C.; Grabowski, J. J. *J. Am. Chem. Soc.* **1992**, *114*, 9663−9664.

(41) Bickelhaupt, F.; Buisman, G.; de Koning, L. J.; Nibbering, N.; Baerends, E. J. *J. Am. Chem. Soc.* **1995**, *117*, 9889−9899.

(42) Flores, A. E.; Gronert, S. *J. Am. Chem. Soc.* **1999**, *121*, 2627−2628.

(43) Gronert, S. *Chem. Rev.* **2001**, *101*, 329−360.

(44) Minato, T.; Yamabe, S. *J. Am. Chem. Soc.* **1988**, *110*, 4586−4593.

(45) Gronert, S. *J. Am. Chem. Soc.* **1991**, *113*, 6041−6048.

(46) Hutter, J.; Alavi, A.; Deutch, T.; Bernasconi, M.; Goedecker, S.; Marx, D.; Tuckerman, M.; Parrinello, M. *CPMD*; MPI für Festkörperforschung and IBM Zurich Research Laboratory: Stuttgart, Germany, 1995−1999.

(47) Hockney, R. W. *Methods Comput. Phys.* **1970**, *9*, 136.

(48) Barnett, R. N.; Landman, U. *Phys. Rev. B* **1993**, *48*, 2081.

(49) Troullier, N.; Martins, J. L. *Phys. Rev. B* **1991**, *43*, 1993−2006.

(50) Kleinman, L.; Bylander, D. M. *Phys. Rev. Lett.* **1982**, *48*, 1425.

(51) Banerjee, A.; Adams, N.; Simons, J.; Shepard, R. *J. Phys. Chem.* **1985**, *89*, 52.

(52) Carter, E.; Ciccotti, G.; Hynes, J.; Kapral, R. *Chem. Phys. Lett.* **1989**, *98*, 472−476.

(53) Sprik, M. *Faraday Discuss.* **1998**, *110*, 437−445.

(54) Paci, E.; Ciccotti, G.; Ferrario, M.; Kapral, R. *Chem. Phys. Lett.* **1991**, *176*, 581−587.

(55) Mülders, T.; Krüger, P.; Swegat, W.; Schlitter, J. *J. Chem. Phys.* **1996**, *104*, 4869−4870.

(56) Nosé, S. *J. Chem. Phys.* **1984**, *81*, 511−519.

(57) Hoover, W. G. *Phys. Rev. A* **1985**, *31*, 1695.

(58) Martyna, G. J.; Klein, M. L.; Tuckerman, M. *J. Chem. Phys.* **1992**, *97*, 2635

(59) Frisch, M. J.; Trucks, G. W.; Schlegel, H. B.; Scuseria, G. E.; Robb, M. A.; Cheeseman, J. R.; Zakrzewski, V. G.; Montgomery, J. A., Jr.; Stratmann, R. E.; Burant, J. C.; Dapprich, S.; Millam, J. M.; Daniels, A. D.; Kudin, K. N.; Strain, M. C.; Farkas, O.; Tomasi, J.; Barone, V.; Cossi, M.; Cammi, R.; Mennucci, B.; Pomelli, C.; Adamo, C.; Clifford, S.; Ochterski, J.; Petersson, G. A.; Ayala, P. Y.; Cui, Q.; Morokuma, K.; Malick, D. K.; Rabuck, A. D.; Raghavachari, K.; Foresman, J. B.; Cioslowski, J.; Ortiz, J. V.; Stefanov, B. B.; Liu, G.; Liashenko, A.; Piskorz, P.; Komaromi, I.; Gomperts, R.; Martin, R. L.; Fox, D. J.; Keith, T.; Al-Laham, M. A.; Peng, C. Y.; Nanayakkara, A.; Gonzalez, C.; Challacombe, M.; Gill, P. M. W.; Johnson, B. G.; Chen, W.; Wong, M. W.; Andres, J. L.; Head-Gordon, M.; Replogle, E. S.; Pople, J. A. *Gaussian 98*, revision A.5; Gaussian, Inc.: Pittsburgh, PA, 1998.

(60) Møller, C.; Plesset, M. *Phys. Rev.* **1934**, *46*, 618.

(61) Nösberger, P.; Bauder, A.; Günthard, H. *Chem. Phys.* **1973**, *1*.

(62) *CRC Handbook of Chemistry and Physics*, 78th ed.; Lide, D., Ed.; CRC Press: Boca Raton, FL, 1997−1998.

(63) Gritsenko, O. V.; Ensing, B.; Shipper, P. R. T.; Baerends, E. J. *J. Phys. Chem. A* **2000**, *104*, 8558−8565.

(64) Murdoch, J. R. *J. Am. Chem. Soc.* **1972**, *94*, 4410−4418.

(65) Raugei, S.; Cardini, G.; Schettino, V. *J. Chem. Phys.* **1999**, *24*, 10887−19894.

(66) Pagliai, M.; Raugei, S.; Cardini, G.; Schettino, V. *J. Chem. Phys.* **2002**, *117*, 2199−2204.

(67) Craig, S. L.; Brauman, J. I. *J. Am. Chem. Soc.* **1999**, *121*, 6690−6699.

(68) Craig, S. L.; Zhong, M.; Brauman, J. I. *J. Am. Chem. Soc.* **1999**, *121*, 11790−11797.

(69) Laaksonen, L. *J. Mol. Graphics* **1992**, *10*, 33−34.

(70) Bergman, D. L.; Laaksonen, L.; Laaksonen, A. *J. Mol. Graphics Modell.* **1997**, *15*, 301−306.